Article:

Tomczyk, AM, Ewertowski, MW and Carrivick, JL orcid.org/0000-0002-9286-5348 (2020) Geomorphological impacts of a glacier lake outburst flood in the high arctic Zackenberg River, NE Greenland. Journal of Hydrology, 591. 125300. ISSN 0022-1694

https://doi.org/10.1016/j.jhydrol.2020.125300

Geomorphological impacts of a glacier lake outburst flood in the high arctic Zackenberg River, NE Greenland

Aleksandra M. Tomczyk[1,2*], Marek W. Ewertowski[1,2], Jonathan L. Carrivick[3]

[1]*Faculty of Geographical and Geological Sciences, Adam Mickiewicz University, Poznań, Poland*
[2]*Department of Environment and Society, Utah State University, Logan, USA*
[3]*School of Geography and water@leeds, University of Leeds, Leeds, UK*

* *Corresponding author: Aleksandra M. Tomczyk, Krygowskiego 10, 61-680 Poznań, Poland, Tel. +48-61-8296-203; e-mail: alto@amu.edu.pl*

Abstract

Glacier outburst floods, (GLOFs), especially those in the arctic, can deliver exceptionally high volumes of sediment and solutes to fjords and shallow-marine settings, in comparison to typical seasonal river flows. These sediments and solutes strongly affect coastal geomorphology and aquatic ecosystems, yet are rarely observed. In this study, we have quantified the short-term geomorphological response of the most distal part of the Zackenberg River, where it enters Young Sund, to a glacier lake outburst flood (GLOF) that occurred on August 6th 2017 in the Zackenberg River, north-east Greenland. The main aims were to: (1) quantify riverbank and floodplain geomorphology changes that occurred as a consequence of the flood; (2) analyse the spatial patterns of those geomorphological changes and suggest the key controls on them. We used a time-series of very high-resolution UAV-generated images taken on the 5th, 6th and 8th of August, which enabled us to compare pre- and post-flood fluvial geomorphology. The GLOF induced intense and widespread geomorphological changes, which was surprising because several floods of a similar magnitude have occurred along this river. Approximately 30 % of the area of interest experienced changes that were larger than the minimum level of detection (0.15 m). Lateral erosion reached almost 10 m in some places. The total volume loss from bank erosion was at least 26,561 m^3 (+/- 14 %), whereas the deposition was at least 7745 m^3 (+/- 39 %). Such an intensive geomorphological response resulted from a combination of factors; namely: (1) bank geometry; (2) composition of bank material; (3) time of occurrence of the event; (4) presence of permafrost; (6) channel geometry; and (7) multitude and diversity of geomorphological processes. We speculate the severity of the geomorphological impact relative to that from previous floods could have been due to warming air temperatures that provided sediment from thawed permafrost, and to an

aggrading delta that raised the river base level. Overall, we contend that climate warming will not only make outburst floods from glaciers more likely but that those floods will achieve more geomorphological work with mechanical erosion of permafrost. Erosion and gravitational failures during future flood events will perhaps become even more widespread and intense.

Keywords: geomorphology; remote sensing; glacier outburst flood; drone; Arctic; hydrology

1. Introduction

Understanding the physical processes that affect river channel morphology and functioning is especially important where rivers are rapidly responding to changing climate and water sources. In the arctic, where climate change is proceeding at some of the fastest rates on Earth, and where glacier meltwater fluxes are supplemented by those from snowmelt and permafrost or groundwater, fluvial geomorphological processes can be divided into: (1) low-magnitude, high-frequency sets of processes (i.e. equilibrium or near-threshold changes); and (2) high-magnitude, low-frequency events (i.e. extreme, catastrophic changes). The latter events are typically difficult to predict and so quantification of geomorphological changes related to them remains very limited compared to the "normal" sets of processes (Tweed and Russell, 1999; Carrivick and Rushmer, 2006, 2009; Tamminga et al., 2015b). Nonetheless, quantification of the geomorphological response of river geomorphology to "extreme" events is key to understanding both its historical evolution (cf. Staines et al., 2015) and for river modelling and monitoring (Tamminga et al., 2015a; Tamminga et al., 2015b) of future water, sediment and solute fluxes (Eybergen and Imeson, 1989; Fryirs, 2013; Magilligan et al., 2015; Naylor et al., 2017; Keesstra et al., 2018).

A geomorphological response to high-magnitude floods can include both erosion of riverbanks and the riverbed, and deposition of sediments. In both cases, river planform and river channel morphology changes, as illustrated in many different geographical settings (e.g. Gardner, 1977; Heritage et al., 2004; Russell et al., 2007; Bucała, 2010; Narama et al., 2010; Wierzbicki et al., 2013; Bangen et al., 2014; Skolasińska et al., 2014; Death et al., 2015; Hajdukiewicz et al., 2015; Nardi and Rinaldi, 2015; Rickenmann et al., 2016; Rinaldi et al., 2016; Wyżga et al., 2016; Emmer, 2017; Naylor et al., 2017; Righini et al., 2017; Cook et al., 2018). Both erosion and deposition affect subsequent river hydraulics, perhaps most importantly channel conveyance and capacity (e.g. Guan et al., 2015; Staines and Carrivick, 2015).

A wide range of techniques have been used to measure bank erosion and channel morphology modifications using different spatial scales with different precision, including erosion metal or electronic pins, bank profilers, planimetric or cross-section topographic survey, as well as GIS-based investigations of historical maps and aerial photographs, (cf. Lawler, 1993; Couper, 2004). However, only recently did advances in the development of portable Unmanned Aerial Vehicles (UAVs or drones) as well as terrestrial and airborne light detection and ranging (LiDAR) systems supported by increasing computational power and structure-from-motion photogrammetry provide us with new tools to be able to monitor and quantify the geomorphological impacts of floods in a rapid, flexible, and detailed manner (Smith et al., 2014; Miřijovský and Langhammer, 2015; Tamminga et al., 2015b; Langhammer and Vacková, 2018; Carrivick and Smith, 2019). These advances expand our ability to infer particular geomorphological processes and their quantity/magnitude responsible for incision, lateral erosion and sedimentation.

The aims of this study are to:

1) Quantify the immediate geomorphological response to a high-magnitude flood event in an arctic river;
2) Investigate the spatial patterns of those geomorphological changes and suggest the key controls on them.

This study achieves these aims through use of high-resolution remote sensing imagery that was collected using a small Unmanned Aerial Vehicle (UAV).

2. Study Area

The study was carried out in the Zackenberg Valley in the high-Arctic setting of northeast Greenland (78°28′12″N; 20°34′23″W) (Figure 1A). Geologically, the region is situated in a north-south orientated fault zone running through Zackenberg and Lindemans valleys, which constitutes the boundary between the Caledonian crystalline basement complexes (Paleoproterozoic gneisses and granitoid rocks with interbedded supracrustal rocks) to the west and Cretaceous sandstones to the east (Henriksen, 2003). More resistant crystalline rocks form high and steep mountain ridges with peaks rising to 1,472 m a.s.l., whereas sandstones build gentle slopes.

The landscape was shaped by glacial, fluvial, marine, and periglacial processes (Gilbert et al., 2017). There are wide U-shaped post-glacial valleys (Lindemansdalen, Zackenbergdalen, Slettedalen, and Store Sødal), deep fiords (Tyrolerfjord and Young Sund) (Figure 1B, C), moraine ridges, and raised delta terraces. Nowadays, the area is not connected with the Greenland Ice Sheet but it was glaciated several times during the Quaternary period (Bennike et al., 2008). Valley glaciers and small ice caps advanced several times during the Holocene but since the Little Ice Age terminus recession, ice surface lowering and consequently ice volume loss has accelerated in recent decades (Carrivick et al., 2019). Permafrost is continuous in the region with an estimated thickness of 200 m to 300 m at the floor of the Zackenberg Valley and 300 m to 500 m in the mountains (Christiansen et al., 2008). The maximum active layer thickness varies spatially from about 0.44 to 0.83 m based on data from the 1997-2014 period (Skov et al., 2017).

From 1996 to 2005, the mean annual air temperature was approximately -9.5°C, with the monthly average temperature ranging from -22.4°C (February) to 5.8°C (July) (Hansen et al., 2008). The mean annual precipitation, falling mostly as snow, was about 260 mm. The vegetation represents white arctic bell-heather (*Cassiope tetragona*), heaths mixed with arctic willow (*Salix arctica*) snow-beds, grasslands, fens, and arctic blueberry (*Vaccinium uliginosum*) (Elberling et al., 2008). Vegetation distribution and density pattern differ according to the altitude, degree of moisture, type of bedrock, and soil properties.

The Zackenberg River catchment covers approximately 514 km^2, roughly 20 % of which is glaciated. Water in the Zackenberg river usually flows from June to October, emanating from the melting of snow, thawing of the upper soil layer, and melting of glacier (Søndergaard et al., 2015). In addition, glacial lake outburst floods (GLOFs), rapid snowmelt, and extreme rain events contribute episodic, sudden-onset and short-lived high-magnitude flows (Kroon et al., 2017). These high-magnitude flows constitute a significant part of the discharge and sediment transport (up to 50 % of the annual sediment discharge - for details, see Hasholt et al. (2008); Søndergaard et al. (2015)). The GLOFs are triggered by drainage of a glacier-dammed lake near the A.P. Olsen Glacier (Figure 1C), which usually occur in July–August (Søndergaard et al., 2015). During GLOFs, water discharge can dramatically increase at up to 400 $m^3 s^{-1}$ (5 % to 10 % of the total annual water discharges), whereas normal discharge in summer usually ranged from 10 $m^3 s^{-1}$ to 60 $m^3 s^{-1}$ according to data for the period between 2009 and 2013 (Søndergaard et al., 2015).

The distal part of the river, where it enters Young Sund, is situated near the mouth of the Zackenberg Valley, next to the Zackenberg Research Station (ZERO). It covers a ~ 2.1 km-long reach where the river cuts through moraines and a raised palaeo-delta ranging in lithology from a diamicton to silts, sands, and gravels (Gilbert et al., 2017). A mixture of sand, gravel and boulders covers the riverbed. The flow pattern is typically turbulent even during relatively small discharges, while the river bed slope (measured at the bridge 2.1 km upstream) is quite steep (1:60) (Ladegaard-Pedersen et al., 2017).

On August 6th, 2017, a glacial lake outburst flood occurred (Figure 2) and the water level in the studied section of the river raised of least 1.6 m in four hours. The flood event lasted approximately 24 h. Although the size of the flood was not very large compared to previous GLOFs, it caused significant changes to the riverscape morphology. Detailed geomorphological maps showing the spatial pattern of the river's immediate geomorphological response to this flood are presented in Tomczyk and Ewertowski (2020).

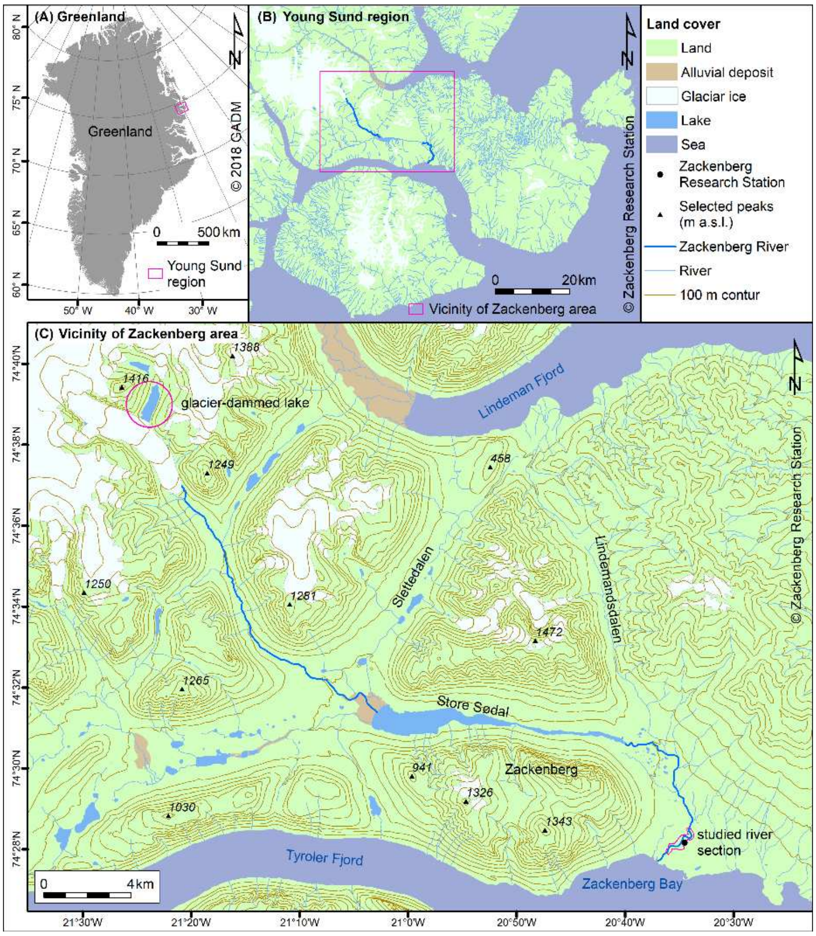

Figure 1. Context maps of the study area: (A) Map of Greenland area with the location of Young Sund region in northeast Greenland highlighted; (B) Map of Young Sund region, with the vicinity of Zackenberg area highlighted; (C) Map of the vicinity of Zackenberg area, with the studied section and glacier-dammed lake highlighted.

Figure 2. An example of low (A and C) and high (B) water levels of the Zackenberg River. In the foreground, it is possible to see a fragment of a bar which was flooded and rebuilt during the flood. In the background, there is an example of the development of debris flow as a result of the riverbank having been undercut by water and permafrost melting. The development of debris flows can threaten the functioning of ZERO station buildings in the long term.

3. Methods

3.1. UAV surveys

To understand the geomorphological response of the Zackenberg river to an extreme flood event, we used time-series of UAV-generated imagery captured immediately before (August 5th - pre-flood dataset), during (August 6th - during-flood dataset), and after (August 8th - post-flood dataset) the 2017 flood. We used a small, lightweight, consumer-grade quadcopter DJI Phantom 4 Pro. The orientation of the models was established using control points (CPs) generated from earlier UAV images from 2014 (COWI, 2015). The UAV surveys and data processing closely followed an operational framework outlined by Ewertowski et al. (2019). Images were processed in Agisoft Metashape 1.5.2 using structure-from-motion photogrammetry, and orthomosaics with a ground sampling distance (GSD) of 1.8 cm to 2.8 cm, and DEMs with GSD of 3.6 to 5.6 cm were produced. Further details about UAV surveys and data processing are presented in Supporting Information.

3.2. Geomorphological Mapping and Geomorphic Change Detection

Geomorphological features were mapped on-screen in ArcMap 10.7. Ground truthing was performed during field works, and the available datasets (e.g. geological and geomorphological maps) were consulted during mapping to ensure proper interpretation of landforms.

A change detection analysis was performed to assess and quantify the efficiency of erosion and deposition. A Geomorphic Change Detection Plugin (Wheaton et al., 2010; Schaffrath et al., 2015) was used in ESRI ArcGIS to construct DEMs of Differences (DoDs), i.e. the values obtained by subtraction of co-registered DEM grid cells. Histograms of elevation differences taken for stable surfaces showed a normal distribution of errors, indicating the non-existence of systematic errors. Based on these histograms, we used a minimum level of detection (minLoD) value of 0.15 m for subsequent DoD analysis, i.e., we assumed spatially uniform errors over the whole DoDs and regarded values below the minLoD as no change.

4. Results

4.1. Results of UAV processing: UAV-generated products and associated challenges

Using a budget ready-to-fly quadcopter, we were able to obtain valuable data and generate high-quality products: digital elevation models and orthomosaics, depicting the situation immediately before (August 5th, 2017), during (August 6th, 2017), and after (August 8th, 2017) the flood. The quality of data was sufficient to investigate the changes in morphology of the river floor and riverbanks.

Despite good overall co-registration, detailed inspection of the DoD revealed that some areas exhibited unexpected values (Figure 3C). Investigation of point clouds and hillshade models indicated that these areas contain height artefacts related to noise in the dense point clouds. All models were therefore manually inspected to identify such artefacts, which were subsequently masked and excluded from further analysis. Other artefacts were related to the water surface which, due to the high turbulence and rapid flow, was not resolved properly through the structure-from-motion (Figure 3D).

DEMs and orthomosaics properly reproduced straight and gentle slopes of the riverbanks. However, overhanging banks posed another problem for monitoring of the flood event's erosional consequences. Despite having taken oblique images, the most severely undercut sections were not represented properly in the digital elevation models nor orthomosaics (Figure 3A, B); therefore, volume of the sediment removed from under these overhung sections were not included in further analysis. In addition, even if visible in orthomosaics, the thickness of the deposition was often relatively low (tens of cm – Figure 6B) and was not included in the volume of detectable changes. Therefore, the volumetric calculations presented in section 4.3 represent minimal values, i.e. they underestimate the full extent of erosion and deposition.

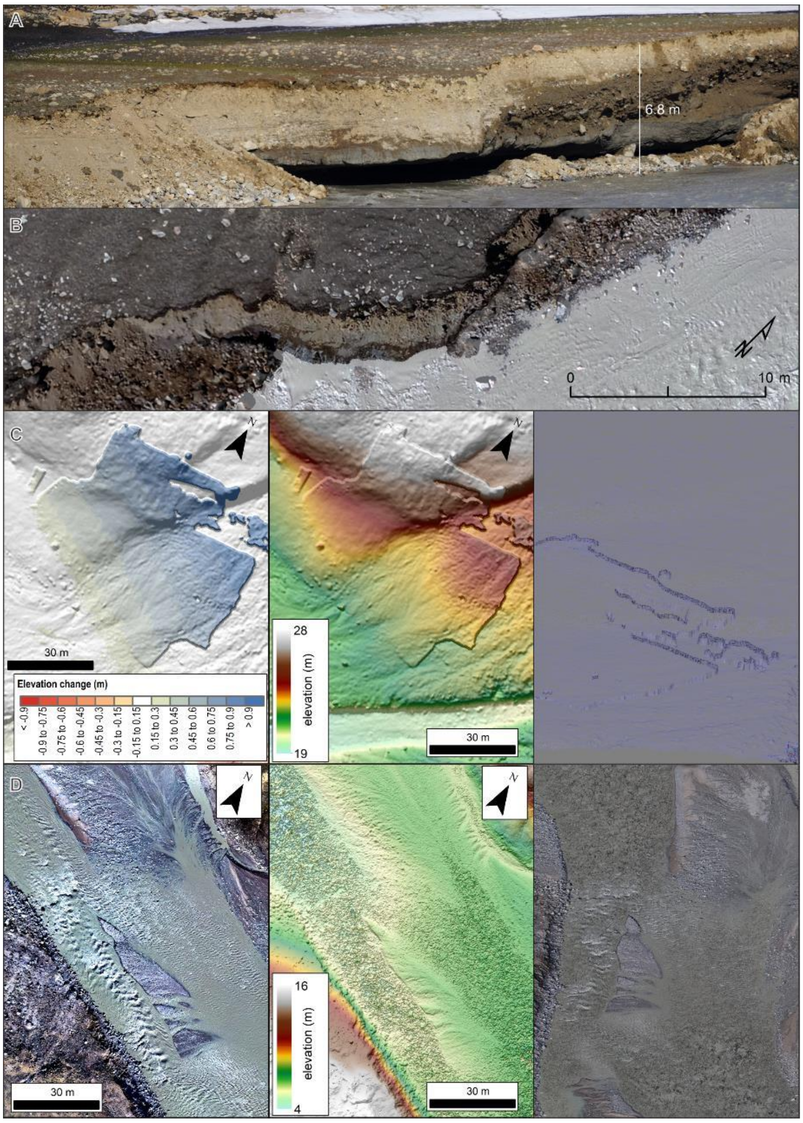

Figure 3. Challenges associated with implementation of UAV surveys for flood monitoring: A, B - Comparison of ground view (A) and aerial view (B) of the undercut riverbanks; C – DEM of Differences showing unexpected deposition (left image), Digital elevation model of corresponding area (central image), mesh of the corresponding are showing artefacts resulting from improper reconstruction of 3D surface (right image); D – orthomosaic of

turbulent section of the river (left image); Digital elevation model (central image) and dense point cloud (right image) of corresponding area showing artefacts caused by water movement.

4.2. Quantification of landscape changes along the river channel as the immediate response to the flood

We studied the 2,155 m reach of the distal Zackenberg River (Figure 4). It is a braided river with one or two main channels split around many bars with sediment particle sizes ranging from fine sands to gravels. The general planform of the river in the studied section is meandering. In the examined section, the river cut through a raised palaeo-delta, which resulted in the development of high (up to 17 m) and steep (43°) slopes and cliffs along the riverbanks.

As the primary focus of this study is to quantify flood-related impacts on the river morphology, we assessed elevation changes within the direct vicinity of the river: bars and riverbanks — this area of interest (AOI) equalled 151,363 m^2. Between the 5th and 8th of August 2017, substantial volume changes were recorded on bars (Section 4.3.) and riverbanks (Section 4.4.). Differentiating DEMs for the whole AOI for this time interval recorded detectable changes (i.e. changes larger than the minimum level of detection: 0.15 m) on 45,243 m^2 (30 % of the AOI). Elevation changes ranged from -11 m to 1.5 m. The area over which surface lowering was recorded equalled 25,333 m^2. The total volume of surface lowering was 26,561 m^3 (+/-14 %), with an average depth of surface lowering at 1.05 m. The total volume of deposition was 7745 m^3 (+/-39 %), with an average thickness of surface rising at 0.4 m. The total net volume difference was -18,816 m^3 (+/-26 %), indicating that erosion was more important than deposition for the studied section of the river. Seventy percent of the AOI data showed no detectable changes – these areas were located on more distant parts of bars and inactive sections of the riverbanks. As mentioned in Section 4.1, the changes presented here are underestimated, mainly due to three reasons: (1) UAV-surveys were not able to capture the undercut sections of sediments; (2) as the water was very turbulent, the structure-from-motion algorithm was not able to properly resolve the level of the water surface; (3) as the suspended sediment concentration was large, the water was not transparent, which unable to estimate the riverbed topography; therefore, our calculation did not include underwater erosion and deposition.

To illustrate the process-form response to the flood, we now present a separate analysis for bars (Section 4.3.) and active bank failures (Section 4.4.).

4.3. Changes to channel and bars morphology

During the flood, the area covered by water (191,207 m^2) more than doubled compared to condition before the flood (87,795 m^2). As a result, most of the mid-channel bars and some of the lateral bars were covered by floodwater. When the river returned to its “normal” discharge after the flood, water covered 96,073 m^2. The width of the river varied before the flood from 16.0 to 97.4 m, during the flood from 46.0 m to 167.8 m, and after the flood from 20.5 to 101.2 m. The average width (measured as active channel area divided by length) changed from 40.74 m before the flood to 88.73 m during the flood, and then to 44.58 m after the flood, which may suggest that the average depth of the channel had decreased.

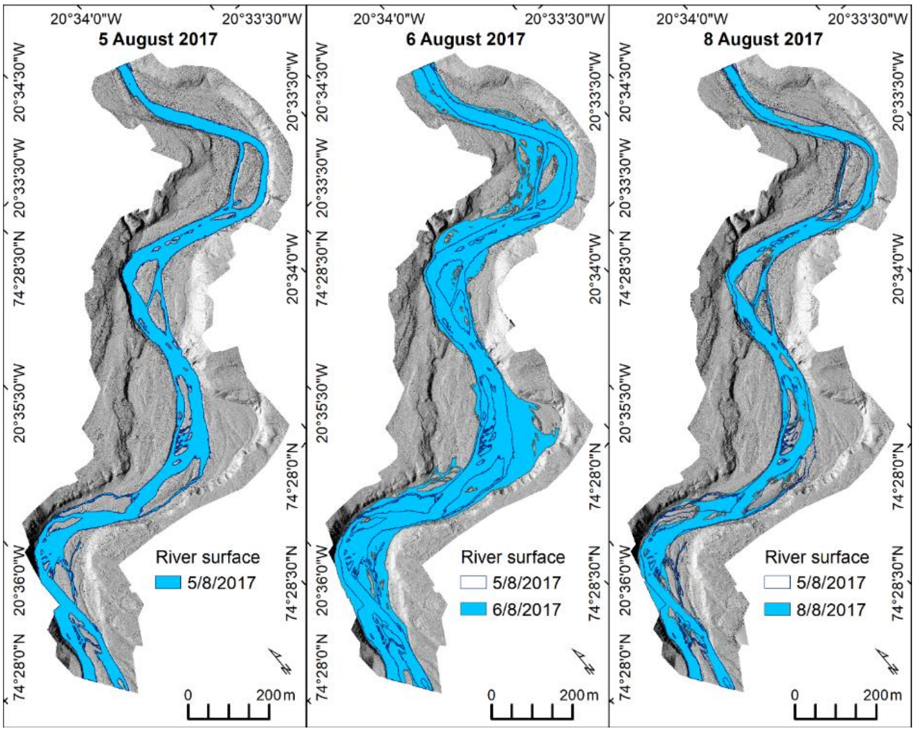

Figure 4. Planform morphology of the Zackenberg River channels before, during, and after the flood

Data showed that between the 5th and 8th of August 2017, the main channel slightly shifted in response to lateral erosion and some bedload deposits became part of the bars by lateral accretion on the inner sides of the channel. Moreover, the surfaces of some larger bars were vertically modified, and new gravel bars developed in the mid-channel positions, indicating areas of higher water flow concentration (Figure 5). The number of individual patches (bars) more than doubled, from 173 before the flood to 373 after the flood, with small, secondary channels appearing between them. Overflow across the bar surfaces left a veneer of fine materials and sands forming ripplemarks (Figure 6). UAV-generated orthomosaics clearly indicate that while sands and fines transport and deposition over the lateral bars were observed, the larger gravel particles remained in the same position despite being underwater during the flood (Figure 6F, G, H). We assumed that most of the eroded material were transported further down the river toward the Zackenberg Bay.

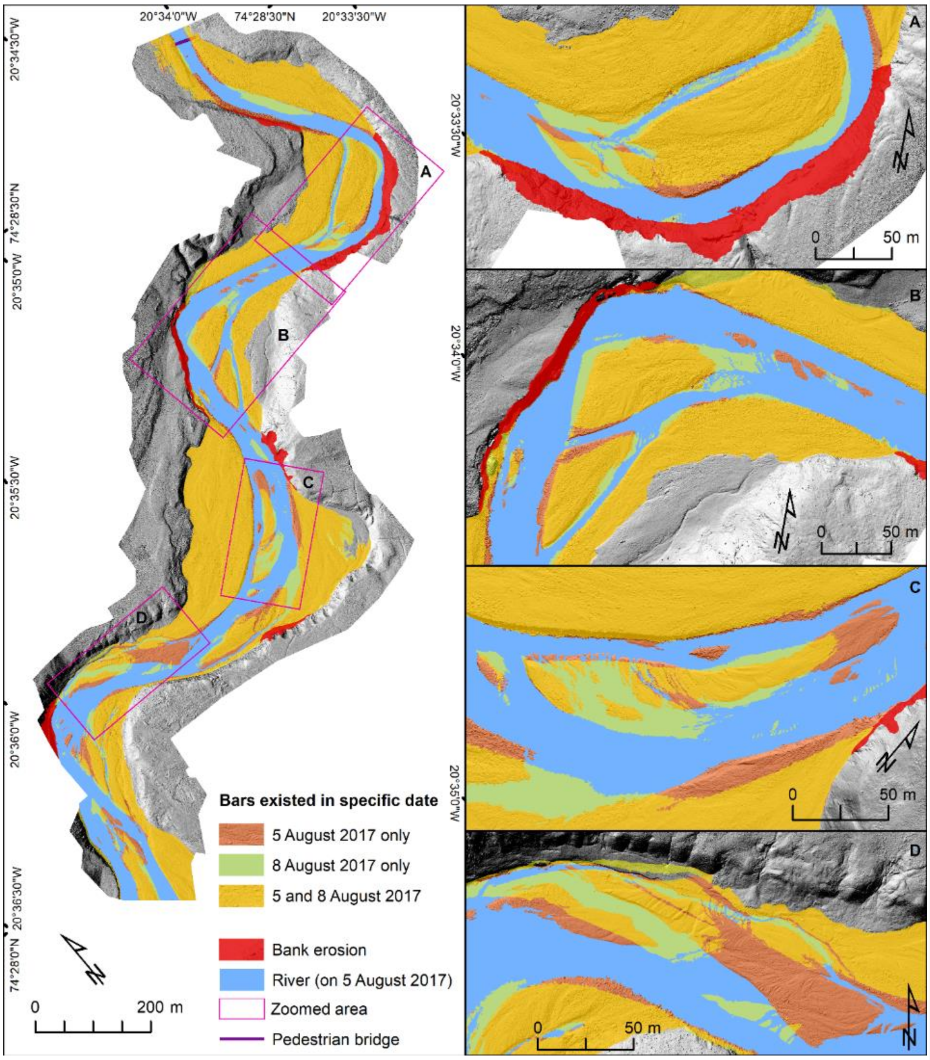

Figure 5. Changes in the shape of bars and floodplains. A, B – examples of mid-channel bars' accretion in both directions: up-river and downriver; C, D – examples of mid-channel bars' migration downriver and edge trimming of lateral bars.

Based on visual analysis of the orthoimages, fresh fluvial material was deposited on 93,702 m^2. This deposition occurred mostly on: (1) existing mid-channel and lateral bars which were already covered by modern fluvial deposits, i.e. on non-vegetated fines, sands, and gravels; (2) freshly created surfaces which developed as a result of the bars' migration (Figures 5 and 6). In addition, a small area of previously vegetated terrain (1,410 m^2) was damaged and then covered by fresh fluvial deposits. In most cases, however, the fresh deposits' veneer was thin (< 0.15 m). As this was lower than the level of detection, most of the deposition was not taken into account in the DoD analysis. The three most important processes of bar transformations are:

1) *Edge trimming (Erosion of bars).* Edge trimming was responsible for the degradation of 9,907 m^2 area covered by bars; on 75 % of this area, erosion was greater than the level of detection (0.15 m). The total volume of eroded material was 3,960 m^3 (+/- 28 %), with an average erosion thickness of 0.54 m. These numbers only accounted for material eroded from the top of the bar surface to the water level (i.e. it did not include any underwater changes).
2) *Deposition of new bars and bar accretion*. As a result of the flood, 8,689 m^2 of new bars were created; on 77 % of this area, deposition was greater than the level of detection (0.15 m). The total volume of recorded deposition was 2,895 m^3 (+/-33 %), with an average deposition thickness of 0.45 m. Similar to the edge trimming, the amount of deposition included only changes from the pre-flood level of the water surface to the post-flood top of the bars.
3) *Remodelling the surfaces of bars existing in both Saturday and Tuesday images.* On the bars which existed in both pre- and post-flood landscape, the total area of detectable changes was 20,655 m^2 (17 % of the total bars' area). Surface lowering was

recorded on 7,385 m^2 of the total bars' area, and the volume of material loss was 2,422 m^3 (+/- 46 %), with an average depth of lowering that equalled 0.33 m. Deposition on the bars was recorded on 13,270 m^2. The volume of deposition equalled 4,793 m^3 (+/- 42 %), while the mean thickness of deposition was 0.36 m. The total net volume difference for preserved bars was 2,372 m^3 (+/-96 %). Such high uncertainty was related to the small values of surface lowering or rising, which were close to the level of detection.

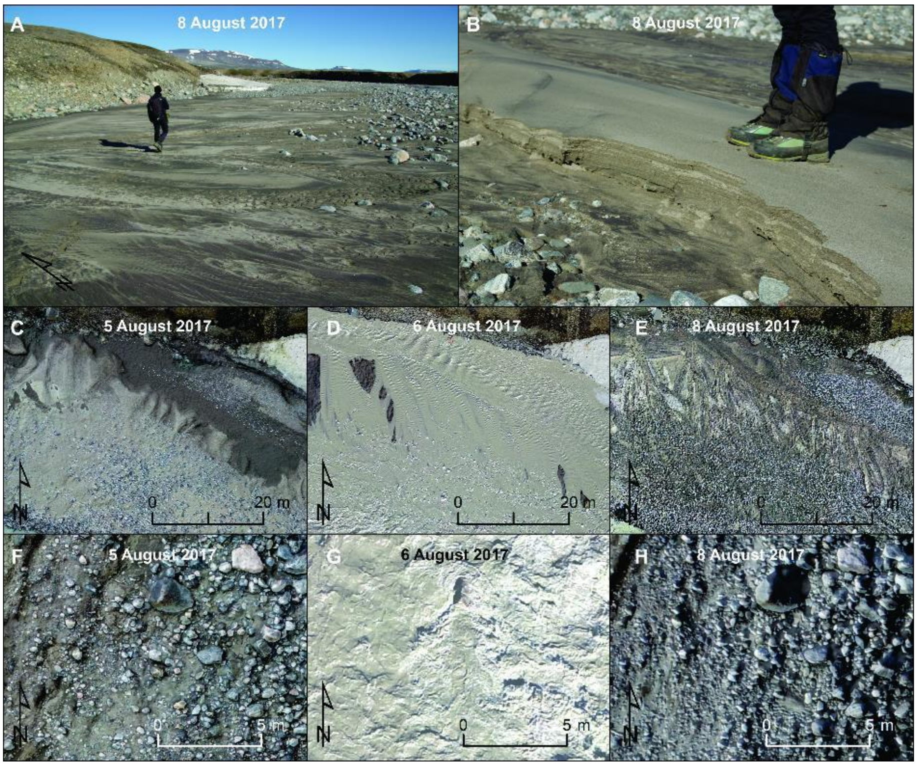

Figure 6. An example of fine-grained flood deposits. Before the flood, this section was covered by fines, sands and gravels (A). During the flood, this area was covered by floodwater (D), which deposited a relatively thin veneer of sediments (A, B, E). The new deposits are clearly visible in the UAV image (E) as well as from the ground (A, C). Note that

the thickness of the fresh deposits was less than 0.2 m (C). Some of the larger clasts did not change their position despite being covered by floodwater during the flood (F, H, G).

4.4. Character and quantification of riverbank erosion

The studied section of the river cut through moraines and elevated late Weichselian delta terraces. Such geomorphological settings have resulted in a steep river profile (0.97 %), the development of steep riverbanks (further enhanced by the presence of permafrost), and domination of lateral erosion of riverbanks. Before the flood, the total length of actively eroded riverbanks (i.e. active mass failures) was 1,729 m (36 % of the total length of both riverbanks which equalled 4,785 m). After the flood, the total length of riverbanks was reduced to 4,659 m, and the active riverbanks to 1,657 m (which was still 36 % of the total after-the-flood length of both riverbanks). This decrease in the banks' length was related to the fact that some sections were straightened as a result of the erosion. Between the 5th and 8th of August 2017, substantial riverbank retreat and volume loss were recorded (Figures 7 and 8) as an immediate response of the riverscape to the flood. The most serious mass failures were observed in six riverbank sections (Figures 7 and 8):

4.4.1 Section 1

The bank of Section 1 (Figure 7A) was composed of diamicton, and while its lower part was frozen, its upper part was an active layer. Dense tundra vegetated the top surface of the bank but its slope was bare. The bank was wet at the top. The bank height before the flood was between 3.3 and 6.4 m, and the slope of this active section was between 16 and 25°. The width of the channel before the flood was about 30 m, which increased during the flood to 50 m. During the flood, the bank was undercut, the riverbed was degraded, and the base of the bank was almost completely cleaned out. The thermo-karst erosion of the riverbank was the most important process contributing to bank degradation. Before the flood, debris flows and debris falls were noticed on the slope. As a result of the flood, and in addition to these processes, debris slides (slumping) were also observed. After the flood, the length of the active bank failure increased from 155 to 180 m. After the flood, the bank's height was similar to that in pre-flood (3.5 – 6.8 m); however, in some places the slope exceeded 90º due to the development of undercut fragments. The top of the bank retreated by up to 9.7 m, and as the deeply undercut section developed, further retreat of the top may be expected. The volume of sediments that eroded from this section was equal to at least 3,587 m^3 (+/-8 %). The maximum lowering of the surface was 4.5 m, while the average lowering was 1.87 m.

4.4.2. Section 2

The bank of Section 2 (Figure 7B) was composed of diamicton (lower part was frozen; upper part an active layer). Sparse tundra vegetated the top of the bank, whereas its slope was bare. The bank's height before the flood ranged from 6.5 to 11 m, while the section slope was between 19 and 43º. The channel width before the flood was about 25 m, which increased during the flood to 142 m, with most basal debris removed. This section comprised two river channels. The main current flowed along the outer channel undercutting the frozen bank. Before the flood debris' sliding (slump), debris flows and debris falls were noticed in the section, with some failure material lying at the toe of the slope. During the flood, lateral erosion (thermo-karst erosion) resulted in the development of an undercut bank. Moreover, debris falls, slides and block falls also occurred. The latter led to the collapse of large blocks (20 m in length) of frozen sediments, which remained at the bottom of the slope after the flood. There were many tension cracks visible at the top surface of the bank, but after the flood, many new cracks appeared, indicating that further collapse of block may yet happen. After the flood, the length of the active section (396 m) and its height (7 – 11 m) were similar to the pre-flood situation. However, the bank slope seriously steepened and, in some places, exceeded 90º due to the presence of undercut fragments. The volume of sediments eroded from this section equalled at least 10,802 m^3 (+/-6 %), as the bank retreated at up to 4.7 m. The maximum depth of lowering was 11 m, while the average lowering was 2.4 m.

4.4.3. Section 3

Section 3 (Figure 7C) was built of diamicton (lower part was frozen; upper part an active layer). Sparse tundra vegetated the top of the bank, whereas the slope was bare. The bank's moisture condition was locally wet. In this part of the river, there were sandy-gravelly bars between three channels of the river. The main channel, situated along the outer bank, was 33 m wide before the flood but increased to 128 m during the flood (as water covered whole bars linking channels). Before the flood, debris slides (slumping) and debris flows were observed on the slope, and a certain amount of failure material was lying at the bank's toe. During the flood, thermo-karst erosion resulted in bank undercutting. Moreover, debris slides, debris falls and debris flows also contributed to bank modification. Locally, some deposits were lying along the toe of the riverbank after the flood. Some tension cracks were visible at the top of the bank; however, no additional tension cracks appeared after the flood. The total length of active failure was the same before and after the flood (221 m). The bank's height was between 3.5 and 7 m before the flood and remained similar after the flood. On the other hand, the bank's slope seriously steepened after the flood. Before the flood, the slope of Section 3 was between 24 and 36º, which then in some places exceeded 90º due to the presence of undercut fragments. The top of the riverbank retreated at up to 4.9 m, while the total volume of sediments removed was 2,699 m^3 (+/-8 %). The maximum depth of surface lowering was 6.5 m, with an average lowering of 2 m.

4.4.4. Section 4

Section 4 (Figure 7D) was built of diamicton (lower part was frozen; upper part an active layer). The section was almost completely bare, and its moisture condition was wet. Some tension cracks were visible at the top of the bank, and a small number of additional cracks appeared after the flood. The main river current flowed close to the right bank. The channel's width ranged from 33 to 50 m before the flood, which widened to between 12 and 64 m after the flood. On August 5th, 2017, two prominent debris flows and some debris falls were observed on the bank. Moreover, at the bank's toe, there were debris-flow deposits in the form of debris lobes, some of which were delivered directly to the water (as indicated by dark brown traces in the water visible in the orthomosaic). The maximum height of the bank before the flood was between 10 and 12.5 m with a moderate slope between 18 and 29º, characteristics that did not change significantly as a result of the flood even though the riverbank retreated by 1.6 m. The total length of the active bank failure was diminished from 404 m to 251 m due to section transformation during the flood by bank undercutting, bed degradation and basal cleanout along with the melting of permafrost and rill erosion. Furthermore, among the six sections described, only this section did not develop any underhanging bank. The total volume of erosion was at least 439 m^3 (+/-28 %), with most of the material deposited at the bank's toe removed. The maximum lowering was 2 m, while the average lowering was 0.53 m.

4.4.5. Section 5

The bank of Section 5 (Figure 7E) was built of stratified sediments: at the bottom was a diamicton, whereas the upper part consisted of silts, sands and gravels. The top of both the bank and slope was bare, while the moisture condition was locally wet. Some tension cracks were observed at the top of the bank while a few new cracks were created during the flood. On August 5^{th}, 2017, the main current flowed for some distance from the riverbank, having been separated by lateral sand and gravel bar. Before the flood, the bank was then modified by debris falls and debris flows. During the flood, as the water level increased, the river current moved toward the bank, causing bank undercutting, bed degradation and basal cleanout. Thermo-karst, snow melting and rill erosion were the most important processes observed in this section. After the flood, some deposits appeared at the bank's toe. Before the flood, the height of the bank ranged from 7 to 12 m, and its slope varied significantly from 10 to 39^{o}. The after-flood morphometry of the bank changed slightly, but remained in a similar range of height and slope values. The length of the active mass failures marginally increased from 487 m (August 5^{th}, 2017) to 493 m (August 8^{th}, 2017), with the dominant processes remaining the same. The bank's retreat was not very high but visible (2.9 m), and some overhanging fragments developed. The volume of removed material was 394 m^3 (+/-25 %), the maximum depth of lowering was 2 m, and the mean lowering was 0.61 m.

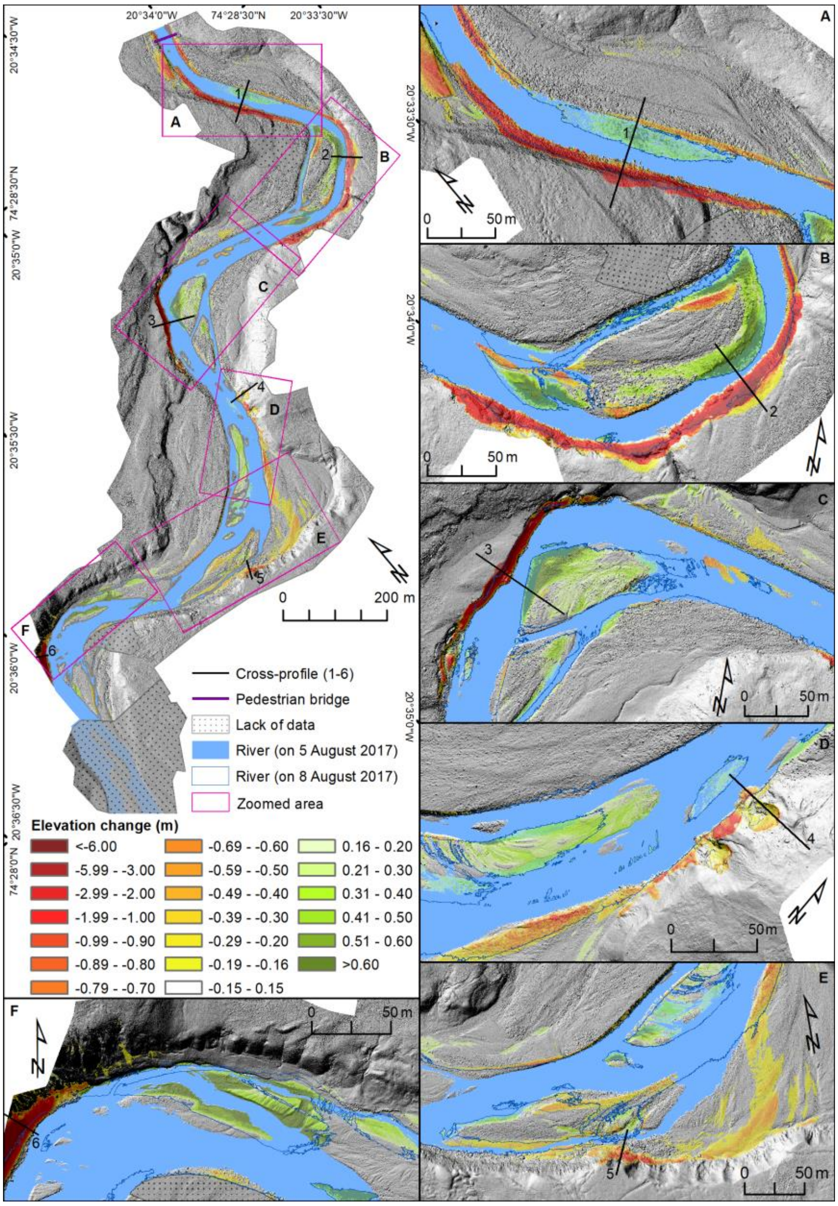

Figure 7. DEM of differences showing the spatial pattern of elevation change distribution along the Zackenberg River. Pink boxes indicate locations of the zoomed area presented in A-F. Black lines mark the locations of cross-profiles presented in Figure 8.

4.4.6. *Section 6*

The bank of Section 6 (Figure 7F) was stratified: diamicton dominated in the bottom part which was overlain by silts, sand and gravels belonging to the elevated palaeo-delta. Sparse tundra vegetated the top of the bank, whereas the slope was bare. The moisture condition was locally wet. Some tension cracks were visible at the top of the riverbank. Before the flood, the river consisted of 2-3 channels, with sandy and gravelly mid-channel bars separating them. The channel flowing close to the bank was relatively narrow (2.2 – 11.7 m) before the flood. Then, as the water level increased, the channel widened to 79 – 159 m. After the flood, it attained a width of 3 to 58 m. On August 5th, 2017, the bank failure included a length of 68 m which increased as a result of the flood to 116 m. There were debris falls and debris flows that developed due to melting of permafrost and snow patches on the riverbank, and there were deposits lying at the bank's toe before the flood. During the flood, the bank was undercut by lateral erosion, in addition to the occurrence of bed degradation and local basal cleanout. This part of the riverbank was high (from 8 to 17 m), and steep (from 24 to 27^{o}), characteristics that remained similar despite the flood (after the flood, the height ranged from 7.5 to 17 m, and the slope was between 24 and 30^{o}). However, the bank was severely undercut, and as a result, the overhanging section developed which could result in cantilever failures. The bank's retreat was up to 5.3 m, with erosion equalling at least 2180 m^3 of material. The maximum thickness of the surface lowering was 6 m, while the mean surface lowering amounted to 1.94 m.

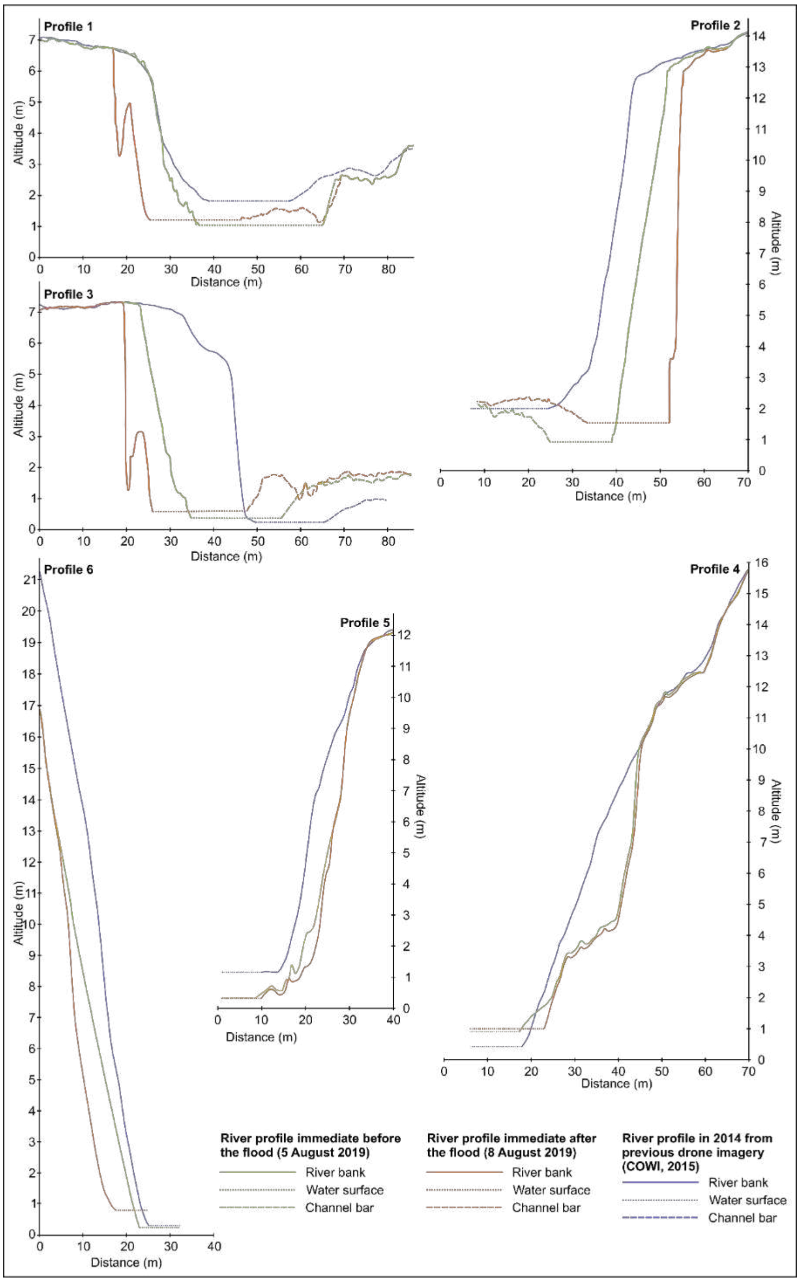

Figure 8. Cross-profiles representing bank's retreat for Sections 1-6. Location of the profiles is shown in Figure 7.

4.5. A comparison of long-term and short-term riverbank changes

We used our UAV-generated data from 2017 (presented in this study) and UAV-generated data from 2014 (COWI, 2015) to compare longer-term changes (2014-2017) with the short-term (2-days 6th August – 8th August 2017) immediate morphological response to a single flood event (Figure 8, Table 1). Elevation changes were investigated in profiles calculated for each of the sections described in 4.4. Our data indicate that, in most sections, the one-day flood in 2017 caused a larger bank erosion than changes in the 2014-2017 period. This situation came about despite the fact that in 2014, 2015 and 2016 the flood had regularly occurred in late summer (July–August) and that the maximum discharges of the Zackenberg River were then higher than during the 2017 flood (Tomczyk and Ewertowski, 2020).

The profile for Section 1 demonstrated that only the bottom part of the slope was modified in the period from 2014 to August 5th, 2017, while the top of the bank remained in the same position. Changes related to the flood being studied (from August 5th to August 8th, 2017) were much larger as the bank retreated even up to 9.7 m (Table 2). A slightly different situation was observed for Sections 2 and 3, where substantial changes between 2014 and August 5th, 2017 were observed - riverbanks retreated at up to 11.6 and 21.6 m, respectively (Figure 8, Table 2). For these sections, the bank's response to the flood in 2017 was also large, equalling 4.7 m and 4.9 m, respectively. Section 4 has been transformed at the bottom and in the middle part of the slope (profile 4) between 2014 and 2017, mainly as a result of debris flow development, which caused retreat of up to 10.2 m between 2014 and August 5th, 2017. The upper part has remained stable. The flood being investigated affected only the bank's toe, which retreated at up to 1.6 m. Profiles in Sections 5 and 6 experienced a moderate retreat between 2014 and August 5th, 2017 (about 6 m), and moderate to relatively small retreat as a result of the flood under investigation (2.9 m and 5.3 m, respectively), which affected mostly the bank's toe.

Table 1. The maximum retreat of the banks in the studied section of the Zackenberg River as an immediate impact of the 2017 flood (two-day changes) compared with previous data from 2014 (COWI, 2015) (three-year changes). Location of the studied profiles is shown in Figure 7.

Section	Maximum retreat during the observation period (meters)	
	Two days (6/08/2017 - 8/08/2017) - this study	Three years (2014 - 2017) - based on previous drone imagery (COWI, 2015)
Section 1	9.7	0
Section 2	4.7	11.6
Section 3	4.9	21.6
Section 4	1.6	10.2
Section 5	2.9	6.1
Section 6	5.3	6.6

5. Discussion

5.1. Factors facilitating bank erosion

Our study has shown changes in the Zackenberg River that were an immediate result of flooding. Even though the size of the 2017 flood was not large compared to long-term trend (Søndergaard et al., 2015), this single event caused some serious changes to the riverbanks and floodplain, with a maximum lateral erosion of almost 10 m, which in some sections was similar to or larger than the previous 3-year bank's retreat (Figure 8, Table 2). Such intensive response was probably the result of a combination of these factors: (1) bank geometry; (2)

composition of bank material; (3) time of occurrence of the event; (4) presence of permafrost; (6) channel geometry; and (7) multitude and diversity of the geomorphological processes:

a) **Bank geometry and geomorphology -** The high (up to 17.0 m before the flood) and steep (up to 43° before the flood) slopes and cliffs along the river facilitated widespread erosion and banks' failures. The steep character of the banks was a consequence of the river cutting through elevated palaeo-delta (which raised about 30 m above the present sea level). The delta consists of a series of terraces, as during sea-level decline in Holocene the river eroded rapidly, to a point where the river is currently cutting the lowest terrace. The delta was built up in the bottom of the valley in the period from the late Weichselian to Holocene (Gilbert et al., 2017).

b) **The composition of bank material** – The riverbanks were composite, including mainly glacial, periglacial and glaciofluvial deposits. The lower riverbanks (up to 2-6 m) comprised of diamicton (sandy, matrix-supported diamicton with clast-supported portions) (Gilbert et al., 2017). Frozen diamicton (linked to the presence of permafrost) was susceptible to undercutting by warmer water causing the retreat of the inundated part of the banks. It could result in overhangs that produce cantilever failures (Luppi et al., 2009). Above the diamicton, there were more resistant silts (up to 1 m thick) and then sands and gravels (Gilbert et al., 2017). Sands and gravels had a loose character and were less resistant. As a result, erosion in the upper part tended to occur grain-by-grain and/or rapidly by mass movements, depending on permafrost occurrence and soil-moisture conditions.

c) **Time of occurrence of the event and the presence of permafrost -** Glacial lake outburst floods in Zackenberg have generally occurred in late summer at the time of maximum soil thaw depth when the bank material is soft, wet and easily eroded. The flood being investigated happened on August 6th, 2017, preceded by an almost two-week period of high air temperatures. As a result, more material was available to erosion and/or mechanical failures under the force of gravity, which led to a significant destabilisation of riverbanks and retreat by large ones. Most probably, this was the reason for significant changes to the riverbanks even though the size of the 2017 flood was not large. Possibly, the pre-GLOF soil conditions produced by thawing permafrost were more important than the magnitude of the GLOF itself.

d) **Channel geometry -** The examined fragment of the river had a meandering character. The erosion was observed along the outer banks of the channel bends, where the flow velocity and shear stress are typically higher.

e) **Multitude and diversity of geomorphological processes** – These processes can be divided into two main groups. The first is entrainment fluvial processes, among which the most important was fluvial thermal erosion, as water warmer than the temperature of the riverbanks came in contact with frozen banks, thereby contributing to a thawing of the frozen sediment and thus facilitating erosion. As a result, the bank material impacted by the thermal processes was subsequently washed away by river currents. This led to the undercutting of the impacted layer of material and could induce cantilever type failures, which typically occur after periods of flood entrainment (Luppi et al., 2009). Other processes of fluvial entrainment included riverbed degradation, incision, and basal cleanout. The second group is gravitational mass failure processes which detach sediment from banks, making it available for further fluvial transport. They comprised debris flow, debris slide (slump), debris fall, and block fall. These two groups of processes were linked, as fluvial entrainment processes (mainly by undercutting riverbank) caused gravitationally induced failures which were also responsible for transporting debris produced by gravitational failures into the river channel. In addition, the creation and widening of pre-existing tension cracks can also contribute to bank erosion due to weakening of the overall stability of slopes at some distance further back from the banks' top. Similar to Grove et al. (2013), Croke et al. (2013) and Thompson et al. (2013), we have noticed that those mass failures, in addition to the fluvial entrainment, significantly impacted the intensity of erosion processes and the volume of sediment supply.

5.2. Impact of GLOF magnitude on geomorphological impacts

Despite there having been at least 14 flood events with peak discharge > 100 m^3/s, which is > five times higher than the long-term mean (summer) discharge, in the Zackenberg river between 1996 and 2018 (Figure 9; Greenland Ecosystem Monitoring Programme: https://data.g-e-m.dk/), the short-term geomorphic response of the 2017 flood was significant (Table 1, Figure 8). For example, in some cases bank erosion was more extensive than during the three years (2014 to 2017). This significant geomorphic impact is perhaps surprising because the severity of flood impacts could be expected to be correlate with flood magnitude.

We can only speculate herein on reasons for this surprising severity of the geomorphological impact of the 2017 flood. We know that there is no temporal pattern in peak discharge (Figure 9), but evaluating whether these floods conform to a flood cycle (Clague and Evan's, 2000) is difficult given the distal position of the river gauge and the likely modification of the flood hydrograph along the flood routeway (c.f. Carrivick et al., 2013). We do not have information about flood volume (at source) or flood duration, so cannot evaluate flood magnitude from either of those metrics. However, outburst flood impacts are not just due to hydraulics, but also to sediment (Carrivick et al., 2004, 2011, 2013; Carrivick, 2007a, b; Carrivick and Rushmer, 2009; Cook et al., 2018). However, modelling of the geomorphological impact of

GLOFs is complex and requires the implementation of hydrodynamic models with integrated sediment transport (Carrivick, 2007a, b; Guan et al., 2015; Staines and Carrivick, 2015). Carrivick et al., 2011). The 2017 flood occurred after a two-week period of unusually warm air temperatures, so meltwater into the ice-dammed lake would have increased and the ice dam itself could have thinned, thereby producing the outburst flood (c.f. Carrivick et al., 2017). However, the warming air temperatures could also have thawed permafrost and destabilised river banks, enabling more geomorphic work to be accomplished than if the ground remained frozen (c.f. Lotsari et al., 2020). Furthermore, it might be considered that the majority of Greenland deltas are aggrading (Bendixen et al. 2017) due to enhanced meltwater generation and sediment mobilisation. It's therefore reasonable to assume that these base level changes are causing rivers across Greenland channels to also be aggrading. Overall, these speculations contend that despite a similar magnitude flood down a river water levels of subsequent floods will become higher, thereby exacerbating geomorphological impact and perhaps also permafrost losses.

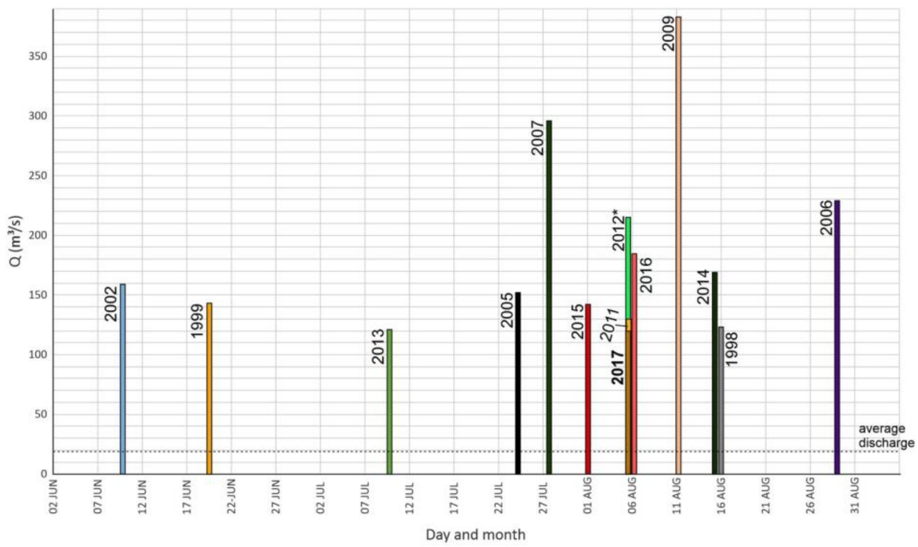

Figure 9. Zackenberg river runoff record of the timing and magnitude of flood event peak discharges compared to the long-term average discharge (1996–2018) (dotted line). Note: the flood in 2012 was so large that it destroyed the hydrological station; therefore, the provided discharge is underestimated. (Figure reproduced from Tomczyk and Ewertowski, 2020).

In comparison to the only other gauged river in Greenland, the maximum water discharges during GLOFs at Zackenberg are generally smaller (from 100 to 400 $m^3 s^{-1}$) (Kroon et al., 2017) than at Watson River (Kangerlussuaq) where the recorded discharges were from 270 to 1430 $m^3 s^{-1}$ (Russell et al., 2011; Mikkelsen et al., 2012; Carrivick et al., 2013). However, GLOFs at Zackenberg have peak discharges that constitute between 5 % to 10 % of the total annual water discharges and 25 % to 50 % the annual sediment discharge (Søndergaard et al., 2015), whereas in Watson River only 0.1 % to 0.7 % of the annual water discharge and from 0.2 % to 1.2 % of the annual sediment and solute discharge (Mikkelsen et al., 2012; Yde et al., 2016; Anderson et al., 2017). Such high disproportion between the average water flow and GLOF discharge in case of the distal part of Zackenberg River might contribute to the severity of the geomorphological response.

5.3. Potential future scenarios

Global climate is getting warmer, especially in the arctic, and as a result permafrost in Greenland is thawing (Anderson et al., 2017). Ongoing global climate warming, which is especially pronounced in the arctic, will probably cause the intensification of GLOF events in terms of both frequency and magnitude (cf. Nardi and Rinaldi, 2015; Carrivick and Tweed, 2016; Harrison et al., 2018). In the period 1991-2005, there was a rise of 2.25 ºC in the annual mean air temperature of the Zackenberg region, and an increase in annual precipitation by 1.9 mm w.eq./year for the period 1958-2005 was estimated (Hansen et al., 2008). The active layer has deepened by more than 1 cm yr^{-1} based on data from the period 1997-2008 (Elberling et al., 2013). Consequently, in the future, there will be more readily available/exposed and unfrozen soil as well as mineral material prone to erosion and/or mechanical, gravitational failures.

Based on our observation, we proposed a model of riverbank erosion on the basis of differences in the four most common situations (Figure 10):

1) Steep slope, strong current, high efficiency of thermal erosion (Figure 10B) – in this situation, highly effective thermal erosion results in the development of overhanging sections. Strong current will likely remove most of the material which fall/slump into a river. Only larger blocks of deposits will be present in a river channel after a flood (Sections 1, 2, 3).
2) Steep slope, moderate current, low efficiency of thermal erosion (Figure 10A) – when slopes are steep, but the efficiency of lateral erosion is lower than in example 1, debris falls and debris slides develop as a result of lateral erosion. Debris may be delivered to a bank's toe, and depending on the strength of the current, they may be removed (section 4) or deposited at a bank's toe (Section 5). If the amount of deposits is large, it may cause an increase in the relative water level.
3) Gentle slope, strong current (Figure 10D) – when pre-flood banks were gentle or flat (usually previous flood deposits and lateral bars), a strong river current would remove the material, sometimes destroying pre-existing vegetation cover as well, but due to the lack of steep topography, no gravitational failures were observed. Examples of this

situation are found in a section of the river next to the bridge at the beginning of Section 1 (Figure 7A) or at the end of Section 4 (Figure 7D).

4) Gentle slope, moderate and weak current (Figure 10C) – in this case, moderate erosion occurred as temporary channels appeared during the flood like at the beginning of Section 5 (Figure 7E). When the flow competence was not sufficient to move larger clasts, these may remain in the same place after the flood (Figure 6) while deposition of fine-grained sediments may occur (Figure 6).

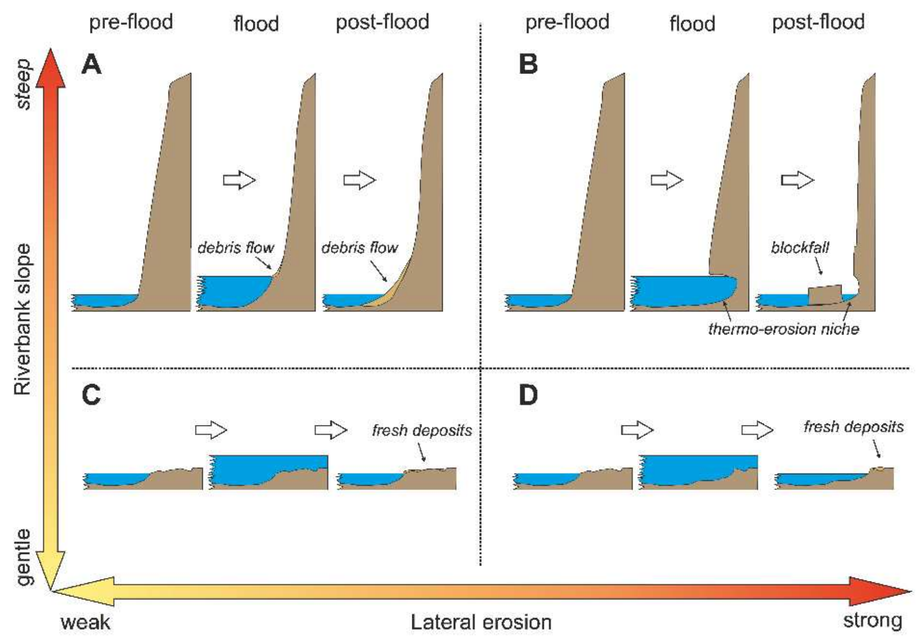

Figure 10. Model of riverbanks' erosion as a consequence of interplay between slope steepens and strength of river current. Further explanation in the text

In addition, the exposure of permafrost as a result of erosion can have two consequences: (1) if the slopes are moderate, debris flow can develop due to increase in the available water on account of the exposed permafrost melts (Section 4); (2) in the case of overhanging slopes, the melting of permafrost will likely result in the falls of sediments and potential collapse of larger blocks. Indeed, the latter situation occurred in Section 2 around late August 2017 (Westergaard-Nielsen et al., 2018).

Future GLOFs and erosion associated with them may have a negative impact on the functioning of the Zackenberg Research Station. The 2017 GLOF damaged that part of the stone banks put up to enforce the bridge (Figure 7). In addition, the development of debris flows in Section 4 might directly threaten station buildings, as further erosion is very likely in the foreseeable future.

6. Conclusions

This study has quantified geomorphological changes to the 2.1 km stretch of the arctic Zackenberg River due to a glacial lake outburst flood (GLOF). We performed surveys immediately before the flood (August 5th, 2017), during the flood (August 6th, 2017), and after the river had returned to its "normal" water level (August 8th, 2017). Such an approach was facilitated by using a UAV platform to obtain high-resolution imagery and the Structure-from-Motion MVS workflow (cf. Carrivick et al., 2016; Smith et al., 2016) to extract extremely detailed topographic data. The short-term geomorphological response was severe; i.e. both intense and extensive, with lateral erosion of ~ 10 m in some places. Approximately 30 % of the area of interest experienced changes that were larger than the minimum level of detection (0.15 m). The total volume loss from bank erosion and edge trimming was at least 26,561 m^3 (+/-14 %), whereas the deposition was at least 7745 m^3 (+/-39 %). Due to limitations described in Section 4.1, such as the presence of overhanging riverbanks and turbulent water flow, the volume of erosion and deposition area was at minimal values, which are more than likely underestimated.

Knowledge about the immediate geomorphological impacts of floods plays a key role in supporting predictive capacity (Tamminga et al., 2015b), understanding the risk of flooding (Cenderelli and Wohl, 2003; Thompson and Croke, 2013), management in terms of warning and protecting society against floods (Hudson et al., 2008; Carrivick and Tweed, 2016). This is especially important when the infrastructure or riverbanks are no longer directly accessible due to flood- or terrain-related hazards. Using a UAV survey for rapid assessment can be beneficial compared to other methods like high-resolution satellite imagery, terrestrial laser scanning (cf. Carrivick et al., 2016; Smith et al., 2016).

Based on our observations, we suggested that the main controls of the response of the riverbanks to the flood event were: channel and bank characteristics (geometry, composition); warm weather condition coupled with the presence of permafrost; and diversity of geomorphological processes contributing to bank erosion. We proposed a conceptual model of the riverbanks' response depending on the steepness of the slope and efficiency of thermal and mechanical erosion of the floodwater.

Future climate changes can cause the intensification of flood events and associated impacts, including delivery of large quantities of freshwater, sediments and solutes into the marine environment (Reynolds, 1998; Harrison et al., 2006; Watanabe et al., 2009; Nardi and Rinaldi, 2015; Carrivick and Tweed, 2016; Harrison et al., 2018). We contend that the geomorphic impact of GLOFs in the arctic is amplified by permafrost (thermal) degradation, and that GLOFs themselves contribute to the mechanical loss of that permafrost. Therefore, documenting the geomorphological records of GLOF events is crucial for the prediction and management of future transformations in the context of upcoming climate changes.

Acknowledgements

Data from the Greenland Ecosystem Monitoring Programme were provided by Asiaq – Greenland Survey, Nuuk, Greenland (ClimateBasis), and the Department of Bioscience, Aarhus University, Denmark in collaboration with Department of Geosciences and Natural Resource Management, Copenhagen University, Denmark (GeoBasis). We are very grateful for the support from INTERACT Network, which allowed us to visit Zackenberg Research Station in 2017. The realisation of the fieldwork would not have been possible without logistic support provided by the crew of the Zackenberg Research Station. The Aleksandra Tomczyk Scholarship at the Utah State University was funded by Polish National Agency for Academic Exchange NAWA within the framework of the Bekker Scholarship Programme (decision number PPN/BEK/2018/1/00381/DEC/1). The preparation of the manuscript was also supported from the internal grant of Faculty of Geographical and Geological Sciences, Adam Mickiewicz University.

Commented [j1]: Just put this is acknowledgements (?)

Disclosure statement

No potential conflict of interest was reported by the authors.

Funding

This work was supported by INTERACT under the European Union H2020 Grant Agreement No.730938, project number: 119 [ArcticFan]

The Aleksandra Tomczyk Scholarship at the Utah State University was funded by Polish National Agency for Academic Exchange NAWA within the framework of the Bekker Scholarship Programme (decision number PPN/BEK/2018/1/00381/DEC/1).

The preparation of the manuscript was also supported from the internal grant of Faculty of Geographical and Geological Sciences, Adam Mickiewicz University.

References

Anderson, N.J. et al., 2017. The Arctic in the Twenty-First Century: Changing Biogeochemical Linkages across a Paraglacial Landscape of Greenland. Bioscience, 67(2): 118-133. DOI:10.1093/biosci/biw158

Bangen, S.G., Wheaton, J.M., Bouwes, N., Bouwes, B., Jordan, C., 2014. A methodological intercomparison of topographic survey techniques for characterizing wadeable streams and rivers. Geomorphology, 206(Supplement C): 343-361. DOI:https://doi.org/10.1016/j.geomorph.2013.10.010

Bendixen, M., Iversen, L.L., Bjørk, A.A., Elberling, B., Westergaard-Nielsen, A., Overeem, I., Barnhart, K.R., Khan, S.A., Box, J.E., Abermann, J. and Langley, K., 2017. Delta progradation in Greenland driven by increasing glacial mass loss. Nature, 550(7674), pp.101-104.

Bennike, O. et al., 2008. Late Quaternary Environmental and Cultural Changes in the Wollaston Forland Region, Northeast Greenland. In: Meltofte, H., Christensen, T.R., lberling, B., Forchhammer, M.C., Rasch, M. (Eds.), Advances in Ecological Research. Academic Press, pp. 45-79. DOI:https://doi.org/10.1016/S0065-2504(07)00003-7

Bucała, A., 2010. Morphological role of floods in the shaping of stream channels in the Gorce mountains (exemplified by Jaszcze and Jamne stream valleys). Geomorphologia Slovaca et Bohemica, 10(1): 45-54.

Carrivick, J.L., 2007a. Hydrodynamics and geomorphic work of jökulhlaups (glacial outburst floods) from Kverkfjöll volcano, Iceland. Hydrol Process, 21(6): 725-740. DOI:10.1002/hyp.6248

Carrivick, J.L., 2007b. Modelling coupled hydraulics and sediment transport of a high-magnitude flood and associated landscape change. Ann Glaciol, 45: 143-154. DOI:10.3189/172756407782282480

Carrivick, J.L. et al., 2019. Accelerated Volume Loss in Glacier Ablation Zones of NE Greenland, Little Ice Age to Present. Geophysical Research Letters, 46(3): 1476-1484. DOI:10.1029/2018GL081383

Carrivick, J.L., Rushmer, E.L., 2006. Understanding high-magnitude outburst floods. Geology Today, 22(2): 60-65. DOI:10.1111/j.1365-2451.2006.00554.x

Carrivick, J.L., Rushmer, E.L., 2009. Inter- and Intra-Catchment Variations in Proglacial Geomorphology: An Example From Franz Josef Glacier and Fox Glacier, New Zealand. Arctic, Antarctic, and Alpine Research, 41(1): 18-36. DOI:10.1657/1523-0430-41.1.18

Carrivick, J.L., Russell, A.J., Tweed, F.S., 2004. Geomorphological evidence for jökulhlaups from Kverkfjöll volcano, Iceland. Geomorphology, 63(1): 81-102. DOI:https://doi.org/10.1016/j.geomorph.2004.03.006

Carrivick, J.L., Smith, M.W., 2019. Fluvial and aquatic applications of Structure from Motion photogrammetry and unmanned aerial vehicle/drone technology. WIREs Water, 6(1): e1328. DOI:10.1002/wat2.1328

Carrivick, J.L., Smith, M.W., Quincey, D.J., 2016. Structure from Motion in the Geosciences. Analytical Methods in Earth and Environmental Science. Wiley-Blackwell, Oxford, UK, 208 pp. DOI:10.1002/9781118895818

Carrivick, J.L., Turner, A.G.D., Russell, A.J., Ingeman-Nielsen, T., Yde, J.C., 2013. Outburst flood evolution at Russell Glacier, western Greenland: effects of a bedrock channel cascade with intermediary lakes. Quaternary Sci Rev, 67: 39-58. DOI:https://doi.org/10.1016/j.quascirev.2013.01.023

Carrivick, J.L., Jones, R. and Keevil, G., 2011. Experimental insights on geomorphological processes within dam break outburst floods. Journal of Hydrology, 408(1-2), pp.153-163.

Carrivick, J.L., Tweed, F.S., 2016. A global assessment of the societal impacts of glacier outburst floods. Global Planet Change, 144: 1-16. DOI:10.1016/j.gloplacha.2016.07.001

Carrivick, J.L., Tweed, F.S., 2019. A review of glacier outburst floods in Iceland and Greenland with a megafloods perspective. Earth-Sci Rev, 196: 102876. DOI:https://doi.org/10.1016/j.earscirev.2019.102876

Cenderelli, D.A., Wohl, E.E., 2001. Peak discharge estimates of glacial-lake outburst floods and "normal" climatic floods in the Mount Everest region, Nepal. Geomorphology, 40(1-2): 57-90.

Cenderelli, D.A., Wohl, E.E., 2003. Flow hydraulics and geomorphic effects of glacial-lake outburst floods in the Mount Everest region, Nepal. Earth Surf Proc Land, 28(4): 385-407. DOI:10.1002/esp.448

Christiansen, H.H., Sigsgaard, C., Humlum, O., Rasch, M., Hansen, B.U., 2008. Permafrost and Periglacial Geomorphology at Zackenberg. In: Meltofte, H., Christensen, T.R., lberling, B., Forchhammer, M.C., Rasch, M. (Eds.), Advances in Ecological Research. Academic Press, pp. 151-174. DOI:https://doi.org/10.1016/S0065-2504(07)00007-4

Clague, J.J. and Evans, S.G., 2000. A review of catastrophic drainage of moraine-dammed lakes in British Columbia. Quaternary Science Reviews, 19(17-18), pp.1763-1783.

Cook, K.L., Andermann, C., Gimbert, F., Adhikari, B.R., Hovius, N., 2018. Glacial lake outburst floods as drivers of fluvial erosion in the Himalaya. Science, 362(6410): 53-57. DOI:10.1126/science.aat4981

Couper, P.R., 2004. Space and Time in River Bank Erosion Research: A Review. Area, 36(4): 387-403.

COWI, 2015. Mapping Greenland's Zackenberg Research Station. https://www.sensefly.com/app/uploads/2017/11/eBee_saves_day_mapping_greenlands_zackenberg_research_station.pdf

Croke, J. et al., 2013. The use of multi temporal LiDAR to assess basin-scale erosion and deposition following the catastrophic January 2011 Lockyer flood, SE Queensland, Australia. Geomorphology, 184: 111-126. DOI:https://doi.org/10.1016/j.geomorph.2012.11.023

Death, R.G., Fuller, I.C., Macklin, M.G., 2015. Resetting the river template: the potential for climate-related extreme floods to transform river geomorphology and ecology. Freshwater Biol, 60(12): 2477-2496.

Desloges, J.R., Church, M., 1992. Geomorphic implications of glacier outburst flooding: Noeick River valley, British Columbia. Canadian Journal of Earth Sciences, 29(3): 551-564.

Elberling, B. et al., 2013. Long-term CO2 production following permafrost thaw. Nature Clim. Change, 3(10): 890-894. DOI:10.1038/nclimate1955

Elberling, B. et al., 2008. Soil and Plant Community-Characteristics and Dynamics at Zackenberg. In: Meltofte, H., Christensen, T.R., lberling, B., Forchhammer, M.C., Rasch, M. (Eds.), Advances in Ecological Research. Academic Press, pp. 223-248. DOI:https://doi.org/10.1016/S0065-2504(07)00010-4

Emmer, A., 2017. Geomorphologically effective floods from moraine-dammed lakes in the Cordillera Blanca, Peru. Quaternary Sci Rev, 177: 220-234. DOI:https://doi.org/10.1016/j.quascirev.2017.10.028

Ewertowski, M.W., Tomczyk, A.M., Evans, D.J.A., Roberts, D.H., Ewertowski, W., 2019. Operational Framework for Rapid, Very-high Resolution Mapping of Glacial Geomorphology Using Low-cost Unmanned Aerial Vehicles and Structure-from-Motion Approach. Remote Sensing, 11(1): 65. DOI:10.3390/rs11010065

Eybergen, F.A., Imeson, A.C., 1989. Geomorphological processes and climatic change. Catena, 16(4): 307-319. DOI:https://doi.org/10.1016/0341-8162(89)90017-9

Fryirs, K., 2013. (Dis)Connectivity in catchment sediment cascades: a fresh look at the sediment delivery problem. Earth Surf Proc Land, 38(1): 30-46. DOI:10.1002/esp.3242

Gardner, J.S., 1977. Some geomorphic effects of a catastrophic flood on the Grand River, Ontario. Canadian Journal of Earth Sciences, 14(10): 2294-2300.

Gilbert, G.L., Cable, S., Thiel, C., Christiansen, H.H., Elberling, B., 2017. Cryostratigraphy, sedimentology, and the late Quaternary evolution of the Zackenberg River delta, northeast Greenland. The Cryosphere, 11(3): 1265-1282. DOI:10.5194/tc-11-1265-2017

Grove, J.R., Croke, J., Thompson, C., 2013. Quantifying different riverbank erosion processes during an extreme flood event. Earth Surf Proc Land, 38(12): 1393-1406. DOI:10.1002/esp.3386

Guan, M., Wright, N.G., Sleigh, P.A., Carrivick, J.L., 2015. Assessment of hydro-morphodynamic modelling and geomorphological impacts of a sediment-charged jökulhlaup, at Sólheimajökull, Iceland. J Hydrol, 530: 336-349. DOI:https://doi.org/10.1016/j.jhydrol.2015.09.062

Hajdukiewicz, H., Wyżga, B., Mikuś, P., Zawiejska, J., Radecki-Pawlik, A., 2015. Impact of a large flood on mountain river habitats, channel morphology, and valley infrastructure. Geomorphology. DOI:http://dx.doi.org/10.1016/j.geomorph.2015.09.003

Hansen, B.U. et al., 2008. Present-day climate at Zackenberg. In: Meltofte, H., Christensen, T.R., lberling, B., Forchhammer, M.C., Rasch, M. (Eds.), Advances in ecological research, pp. 111-149.

Harrison, S. et al., 2006. A glacial lake outburst flood associated with recent mountain glacier retreat, Patagonian Andes. Holocene, 16(4): 611-620. DOI:Doi 10.1191/0959683606hl957rr

Harrison, S. et al., 2018. Climate change and the global pattern of moraine-dammed glacial lake outburst floods. The Cryosphere, 12(4): 1195-1209. DOI:10.5194/tc-12-1195-2018

Hasholt, B. et al., 2008. Hydrology and Transport of Sediment and Solutes at Zackenberg, Advances in Ecological Research. Academic Press, pp. 197-221. DOI:https://doi.org/10.1016/S0065-2504(07)00009-8

Henriksen, N., 2003. Caledonian orogen East Greenland 70°-82° - Geological Map 1:1 000 000. In: Higgins, A.K. (Ed.). The Geological Survey of Denmark and Greenland, Copenhagen, Denmark.

Heritage, G.L., Large, A.R.G., Moon, B.P., Jewitt, G., 2004. Channel hydraulics and geomorphic effects of an extreme flood event on the Sabie River, South Africa. Catena, 58(2): 151-181. DOI:https://doi.org/10.1016/j.catena.2004.03.004

Hudson, P.F., Middelkoop, H., Stouthamer, E., 2008. Flood management along the Lower Mississippi and Rhine Rivers (The Netherlands) and the continuum of geomorphic adjustment. Geomorphology, 101(1): 209-236. DOI:https://doi.org/10.1016/j.geomorph.2008.07.001

Keesstra, S. et al., 2018. The way forward: Can connectivity be useful to design better measuring and modelling schemes for water and sediment dynamics? Sci Total Environ, 644: 1557-1572. DOI:https://doi.org/10.1016/j.scitotenv.2018.06.342

Kroon, A. et al., 2017. Deltas, freshwater discharge, and waves along the Young Sound, NE Greenland. Ambio, 46(Suppl 1): 132-145. DOI:10.1007/s13280-016-0869-3

Ladegaard-Pedersen, P. et al., 2017. Suspended sediment in a high-Arctic river: An appraisal of flux estimation methods. Science of The Total Environment, 580: 582-592. DOI:https://doi.org/10.1016/j.scitotenv.2016.12.006

Langhammer, J., Vacková, T., 2018. Detection and Mapping of the Geomorphic Effects of Flooding Using UAV Photogrammetry. Pure and Applied Geophysics, 175(9): 3223-3245. DOI:10.1007/s00024-018-1874-1

Lawler, D.M., 1993. The measurement of river bank erosion and lateral channel change: A review. Earth Surf Proc Land, 18(9): 777-821. DOI:10.1002/esp.3290180905

Lotsari, E., Hackney, C., Salmela, J., Kasvi, E., Kemp, J., Alho, P. and Darby, S.E., 2020. Sub-arctic river bank dynamics and driving processes during the open-channel flow period. Earth Surface Processes and Landforms, 45(5), pp.1198-1216.

Luppi, L., Rinaldi, M., Teruggi, L.B., Darby, S.E., Nardi, L., 2009. Monitoring and numerical modelling of riverbank erosion processes: a case study along the Cecina River (central Italy). Earth Surf Proc Land, 34(4): 530-546. DOI:10.1002/esp.1754

Magilligan, F.J., Buraas, E.M., Renshaw, C.E., 2015. The efficacy of stream power and flow duration on geomorphic responses to catastrophic flooding. Geomorphology, 228: 175-188. DOI:https://doi.org/10.1016/j.geomorph.2014.08.016

Mikkelsen, A.B., Hasholt, B., Knudsen, N.T., Nielsen, M.H., 2012. Jökulhlaups and sediment transport in Watson River, Kangerlussuaq, West Greenland. Hydrol Res, 44(1): 58-67. DOI:10.2166/nh.2012.165

Miřijovský, J., Langhammer, J., 2015. Multitemporal Monitoring of the Morphodynamics of a Mid-Mountain Stream Using UAS Photogrammetry. Remote Sensing, 7(7): 8586-8609.

Narama, C., Duishonakunov, M., Kaab, A., Daiyrov, M., Abdrakhmatov, K., 2010. The 24 July 2008 outburst flood at the western Zyndan glacier lake and recent regional changes in glacier lakes of the Teskey Ala-Too range, Tien Shan, Kyrgyzstan. Nat Hazard Earth Sys, 10(4): 647-659.

Nardi, L., Rinaldi, M., 2015. Spatio-temporal patterns of channel changes in response to a major flood event: the case of the Magra River (central–northern Italy). Earth Surf Proc Land, 40(3): 326-339. DOI:10.1002/esp.3636

Naylor, L.A. et al., 2017. Stormy geomorphology: geomorphic contributions in an age of climate extremes. Earth Surf Proc Land, 42(1): 166-190. DOI:10.1002/esp.4062

Reynolds, J.M., 1998. High-altitude glacial lake hazard assessment and mitigation: a Himalayan perspective. Geol Soc Eng Geol Sp(15): 25-34. DOI:https://doi.org/10.1144/GSL.ENG.1998.015.01.03

Rickenmann, D., Badoux, A., Hunzinger, L., 2016. Significance of sediment transport processes during piedmont floods: the 2005 flood events in Switzerland. Earth Surf Proc Land, 41(2): 224-230. DOI:10.1002/esp.3835

Righini, M. et al., 2017. Geomorphic response to an extreme flood in two Mediterranean rivers (northeastern Sardinia, Italy): Analysis of controlling factors. Geomorphology, 290: 184-199. DOI:https://doi.org/10.1016/j.geomorph.2017.04.014

Rinaldi, M. et al., 2016. An integrated approach for investigating geomorphic response to extreme events: methodological framework and application to the October 2011 flood in the Magra River catchment, Italy. Earth Surf Proc Land, 41(6): 835-846. DOI:10.1002/esp.3902

Russell, A.J., Carrivick, J.L., Ingeman-Nielsen, T., Yde, J.C., Williams, M., 2011. A new cycle of jökulhlaups at Russell Glacier, Kangerlussuaq, West Greenland. J Glaciol, 57(202): 238-246. DOI:10.3189/002214311796405997

Russell, A.J., Gregory, A.R., Large, A.R.G., Fleisher, P.J., Harris, T.D., 2007. Tunnel channel formation during the November 1996 jokulhlaup, Skeioararjokull, Iceland. Ann Glaciol, 45: 95-103.

Russell, A.J. et al., 2010. An unusual jökulhlaup resulting from subglacial volcanism, Sólheimajökull, Iceland. Quaternary Sci Rev, 29(11): 1363-1381. DOI:https://doi.org/10.1016/j.quascirev.2010.02.023

Schaffrath, K.R., Belmont, P., Wheaton, J.M., 2015. Landscape-scale geomorphic change detection: Quantifying spatially variable uncertainty and circumventing legacy data issues. Geomorphology, 250(Supplement C): 334-348. DOI:https://doi.org/10.1016/j.geomorph.2015.09.020

Skolasińska, K., Szczuciński, W., Mitręga, M., Jagodziński, R., Lorenc, S., 2014. Sedimentary record of 2010 and 2011 Warta River seasonal floods in the region of Poznań, Poland. Geol Q, 59(1): 47-60.

Skov, K. et al., 2017. Zackenberg basic: The ClimateBasis and GeoBasis programme, Denmark.

Smith, M.W., Carrivick, J.L., Hooke, J., Kirkby, M.J., 2014. Reconstructing flash flood magnitudes using 'Structure-from-Motion': A rapid assessment tool. J Hydrol, 519: 1914-1927. DOI:https://doi.org/10.1016/j.jhydrol.2014.09.078

Smith, M.W., Carrivick, J.L., Quincey, D.J., 2016. Structure from motion photogrammetry in physical geography. Progress in Physical Geography: Earth and Environment, 40(2): 247-275. DOI:10.1177/0309133315615805

Søndergaard, J. et al., 2015. Mercury exports from a High-Arctic river basin in Northeast Greenland (74°N) largely controlled by glacial lake outburst floods. Sci Total Environ, 514: 83-91. DOI:https://doi.org/10.1016/j.scitotenv.2015.01.097

Staines, K.E.H., Carrivick, J.L., 2015. Geomorphological impact and morphodynamic effects on flow conveyance of the 1999 jökulhlaup at sólheimajökull, Iceland. Earth Surf Proc Land, 40(10): 1401-1416. DOI:10.1002/esp.3750

Staines, K.E.H. et al., 2015. A multi-dimensional analysis of pro-glacial landscape change at Sólheimajökull, southern Iceland. Earth Surf Proc Land, 40(6): 809-822. DOI:10.1002/esp.3662

Tamminga, A., Hugenholtz, C., Eaton, B., Lapointe, M., 2015a. Hyperspatial remote sensing of channel reach morphology and hydraulic fish habitat using an unmanned aerial vehicle (UAV): A first assessment in the context of river research and management. River Res Appl, 31(3): 379-391.

Tamminga, A.D., Eaton, B.C., Hugenholtz, C.H., 2015b. UAS-based remote sensing of fluvial change following an extreme flood event. Earth Surf Proc Land, 40(11): 1464-1476.

Thompson, C., Croke, J., 2013. Geomorphic effects, flood power, and channel competence of a catastrophic flood in confined and unconfined reaches of the upper Lockyer valley, southeast Queensland, Australia. Geomorphology, 197: 156-169. DOI:https://doi.org/10.1016/j.geomorph.2013.05.006

Thompson, C., Croke, J., Grove, J., Khanal, G., 2013. Spatio-temporal changes in river bank mass failures in the Lockyer Valley, Queensland, Australia. Geomorphology, 191: 129-141. DOI:https://doi.org/10.1016/j.geomorph.2013.03.010

Tomczyk, A.M., Ewertowski, M.W., 2020. UAV-based remote sensing of immediate changes in geomorphology following a glacial lake outburst flood at the Zackenberg river, northeast Greenland. J Maps, 16(1): 86-100. DOI:10.1080/17445647.2020.1749146

Tweed, F.S., Russell, A.J., 1999. Controls on the formation and sudden drainage of glacier-impounded lakes: implications for jökulhlaup characteristics. Progress in Physical Geography: Earth and Environment, 23(1): 79-110. DOI:10.1177/030913339902300104

Watanabe, T., Lamsal, D., Ives, J.D., 2009. Evaluating the growth characteristics of a glacial lake and its degree of danger of outburst flooding: Imja Glacier, Khumbu Himal, Nepal. Norsk Geogr Tidsskr, 63(4): 255-267. DOI:10.1080/00291950903368367

Westergaard-Nielsen, A. et al., 2018. Spatial data on: allows for quantification of. In: Christensen, T.R., Topp-Jørgensen, E. (Eds.), Greenland Ecosystem Monitoring Annual Report Cards 2017. Danish Centre for Environment and Energy, Aarhus University, Denmark, pp. 44 pp.

Wheaton, J.M., Brasington, J., Darby, S.E., Sear, D.A., 2010. Accounting for uncertainty in DEMs from repeat topographic surveys: improved sediment budgets. Earth Surf Proc Land, 35(2): 136-156. DOI:10.1002/esp.1886

Wierzbicki, G., Ostrowski, P., Mazgajski, M., Bujakowski, F., 2013. Using VHR multispectral remote sensing and LIDAR data to determine the geomorphological effects of overbank flow on a floodplain (the Vistula River, Poland). Geomorphology, 183(0): 73-81. DOI:http://dx.doi.org/10.1016/j.geomorph.2012.06.020

Wyżga, B., Zawiejska, J., Radecki-Pawlik, A., 2016. Impact of channel incision on the hydraulics of flood flows: Examples from Polish Carpathian rivers. Geomorphology. DOI:http://dx.doi.org/10.1016/j.geomorph.2015.05.017

Yde, J.C. et al., 2016. Stable oxygen isotope variability in two contrasting glacier river catchments in Greenland. Hydrol. Earth Syst. Sci., 20(3): 1197-1210. DOI:10.5194/hess-20-1197-2016